J Inorg Organomet Polym (2015) 25:293–300
DOI 10.1007/s10904-014-0144-7

Bioinspired Nanoarchitectonics of Naphthalene Diimide to Access 2D Sheets of Tunable Size, Shape, and Optoelectronic Properties

M. Pandeeswar · T. Govindaraju

Received: 10 October 2014 / Accepted: 9 December 2014 / Published online: 17 December 2014

Abstract A bioinspired nanoarchitectonics design strategy is adapted to construct 2D sheets of promising n-type organic semiconductor naphthalene diimide (NDI) with tunable size, shape and optoelectronic properties. Modulation of noncovalent interactions such as intermolecular NDI–NDI aromatic and hydrogen bonding interactions among the molecules within the self-assembled 2D sheets is achieved by the minute structural mutations on the NDI imide substitutions in the form of glycine derivatives (carboxylic acid, amide and ester). Microscopy studies (FESEM and AFM) showed the formation of flat, smooth and large 2D nanosheets with distinct lateral and height profiles. Photophysical studies revealed unique solid state optoelectronic properties with promising temperature responsive fluorescence behavior with quite longer life time values which are useful as temperature sensor materials. The concentration and temperature dependent ^{1}H NMR and IR studies provided the insights into distinct noncovalent interactions responsible for the observed NDI 2D sheets with variable size and shape. Furthermore, PXRD studies revealed highly crystalline molecular organization within the 2D sheets. On account of these tunable unique properties, the 2D sheets derived from NDI-conjugates might find a wide range of future interdisciplinary applications from materials to biomedicine.

Keywords 2D Nanoarchitectonics · Bioinspired strategy · Aromatic interactions · Hydrogen bonding · Optoelectronic

1 Introduction

Nanoarchitectonics an emerging area of an interdisciplinary nature attracting a great deal of interest owing to fascinating structural and functional features, in both scientific and technological research [1–5]. In particular, 2D nanoarchitectonics deals with 2D nanostructures with large specific surface area and facets [1–7]. They exhibit exceptional electrical, mechanical, thermal and optical properties desirable for nano(bio)technology, storage, optical, dielectric and electronics, catalysis, sensing, separation, optoelectronics, biomaterials, membranes, and energy storage and conversion related applications [1–32]. Graphene has been one of the most fascinating 2D nanomaterials in the area of 2D nanoarchitectonics [6, 7]. In recent times, 2D inorganic nanomaterials namely metal nanosheets, metal oxide/sulfide/selenide nanosheets, perovskite sheets, zeolites and hybrid materials, received remarkable attention owing to their high chemical, thermal stabilities and wide-band-gap semiconducting properties [8–14]. The soft organic and hybrid materials based 2D nanoarchitectonics is relatively young but exhibit promising multidisciplinary applications and therefore attracting a great deal of attention from the scientific community around the globe [1–5, 15–32]. Substantial efforts have been devoted to obtain the 2D nanoarchitectures via both top down and bottom up approaches such as exfoliation of layered crystals, templating at the liquid/air, liquid/liquid and liquid/solid interfaces, chemical vapor deposition, self-assembly and chemical synthesis [1–5, 15–32]. There are

Electronic supplementary material The online version of this article (doi:10.1007/s10904-014-0144-7) contains supplementary material, which is available to authorized users.

M. Pandeeswar · T. Govindaraju (✉)
Bioorganic Chemistry Laboratory, New Chemistry Unit, Jawaharlal Nehru Centre for Advanced Scientific Research, Jakkur P.O., Bengaluru 560064, India
e-mail: tgraju@jncasr.ac.in

few reports on organic 2D nanoarchitectonics in the literature based on biomacromolecules and synthetic polymers through supramolecular design principles with limited scope and applications owing to their low yields, large molecular size, low stability, lack of long-range order, narrow operating conditions, high cost associated with the processes [15–30]. Interestingly, 2D organic semiconducting nanoarchitectonics have been emerged as promising molecular organizations in organic field effect transistor applications by displaying high field effect mobilities via increased intermolecular interactions with neighboring molecules which preserves the 2D molecular order [31, 32]. However direct control of noncovalent interactions in n-type organic semiconductor molecular organization into well-defined 2D nanoarchitectonics remains a key daunting challenge in organic electronics. We have been extensively working in the area of organic nanoarchitectonics which is based on adapting bioinspired approach to understand the design principles as well as to develop 1D and 2D nanomaterials for applications in organic electronics, biomaterials and biomedicine [22–24, 26, 27, 42, 43].

Naphthalene diimide (NDI) and its derivatives are extensively studied class of n-type organic semiconducting materials [33–35]. On account of the novel characteristics like molecular planarity, high π-acidity, high melting points, high tendency to aggregation through π–π stacking interactions, excellent chemical, thermal, photochemical stabilities, well-defined redox behaviour and tunable optoelectronic properties (absorbance and emission), NDIs received special interest in biological, biomedical, materials science and supramolecular chemistry [36–49]. NDI derivatives have been used as intercalators of DNA, chemotherapy, conducting materials, optical brighteners, electro-photography, fluorescent labelling systems, metalomacrocycles, models for the photosynthetic reaction centre, sensors and anticancer agents [36–49]. During the past few years, various bioinspired and abiotic design strategies were employed to realize the nanomaterials of NDIs with diverse structural, chemical and physical properties [36–49]. Recently, for the first time we reported the amino acid conjugated NDI derivatives and their self-assembly into 2D nanosheets with tunable optical properties [22–24, 26]. The fabrication of 2D nanostructures of NDI with precisely tailored size, shape and properties is still in its infancy owing to the difficulty in controlling the intermolecular noncovalent interactions [1–5].

Nature meticulously employs biomolecules such as amino acids for designing complex biological systems and materials. It should be noted that amino acids exhibit remarkable structure–property correlations, selectivity, specificity and complexity. A bioinspired approach can be envisaged to exploit the extraordinary properties of amino acids in the development of new biomimetic materials with novel functional properties [1–5]. In such a design strategy, minute structural mutations in the form of amino acid derivatives play key role in controlling the intermolecular noncovalent interactions and subsequent molecular organization. Herein we report the bioinspired fine tuning of NDI molecular organization into 2D nanostructures with well-defined size, shape and optoelectronic properties by controlling the intermolecular noncovalent interactions such as aromatic and hydrogen bonding interactions. Aromatic and hydrogen bonding interactions play a key role and are critical for various biological processes, for example, DNA helix formation, RNA recognition, stabilization of proteins and peptide secondary structures and enzymatic action among others. With this in mind, we selected a simple amino acid glycine (**1**) and its derivatives glycine methylester (**2**) and glycinamide (**3**) as imide substituents on NDI to induce differential self-assembly properties through variable intermolecular hydrogen bonding (Fig. 1). Remarkably, the designed NDI bolaamphiphiles (**1**, **2** and **3**) were found to self-assembly into 2D nanoarchitectures with distinct size, shape and optoelectronic properties via aromatic interactions induced by central planar, π-electron deficient NDI core and distinct intermolecular hydrogen bonding interactions introduced by the glycine derivatives (**1**: carboxylic acid, **2**: amide and **3**: methyl ester) as shown in Fig. 1.

2 Results and Discussion

NDI bolaamphiphiles **1**–**3** were synthesized by the condensation of corresponding glycine, glycinamide and glycinemethylester with the 1,4,5,8-naphthalenetetracarboxylic dianhydride (NDA), in good yields (>80 %). All the NDI bolaamphiphiles (**1**–**3**) were characterized by NMR spectroscopy and elemental analysis. NDI conjugates (**1**, **2** and **3**) were found to be readily soluble in dimethyl sulfoxide (DMSO). To induce the self-assembly of NDIs **1**–**3** through hydrophobic effect we chose to perform our spectroscopic and microscopy studies in aqueous solution (H_2O/DMSO; 80/20, v/v).

2.1 Morphological Studies

Field emission scanning electron microscopy (FESEM) images of **1**, **2** and **3** revealed the presence of well-ordered flat and distinct laterally extended 2D sheets (Fig. 2). **1** displayed the formation of large laterally extended 2D sheets with average length and width is in the range of 5–10 μm (Fig. 2a). Furthermore, self-assembly of **2** and **3** led to the formation of rectangular sheets with different aspect ratios. 2D sheets with 20–30 μm length and 3–5 μm

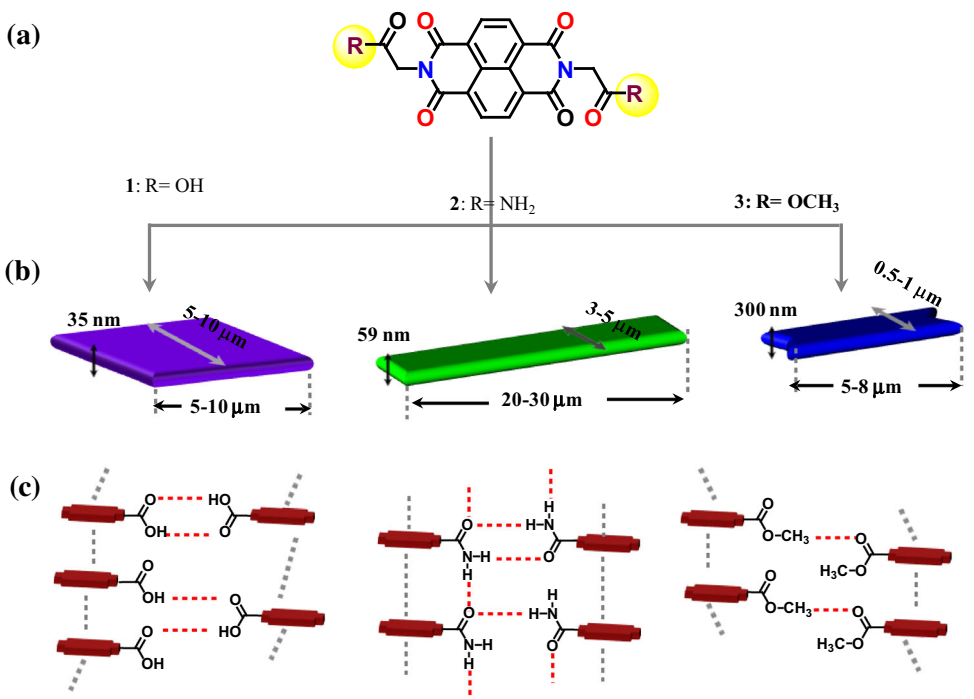

Fig. 1 **a** Molecular structures of glycine and its derivatives conjugated NDIs **1**, **2** and **3**. **b** Schematic representation of 2D sheets and their dimensions. **c** Proposed noncovalent intermolecular interactions, hydrogen bonding (*red dash line*) and NDI–NDI aromatic interactions (*black dash line*) present in 2D sheets. (Color figure online)

width were observed in case of **2** (Fig. 2b), whereas **3** formed relatively smaller 2D sheets with 5–8 µm length and 0.5–1 µm width (Fig. 2c). Atomic force microscopy (AFM) studies were employed to measure the height profiles of 2D sheets of **1**, **2** and **3** (Fig. 2d–f). AFM micrograph showed relatively smooth and flat 2D nanosheets with average single layer thickness of 35, 59 and 300 nm for **1**, **2** and **3** respectively (Fig. 2g–i). The sheets of **1**, **2** and **3** exhibited thermal reversibility by displaying their 2D architecture even after annealing to 100 °C (Figure S13).

2.2 Photophysical Studies

The mode of aromatic interactions within the 2D nanosheets was explored through UV–vis absorption and fluorescence emission spectroscopic measurements (Fig. 3). UV–vis absorption spectra of **1**, **2** and **3** in DMSO displayed vibronically well-resolved sharp bands in the 300–400 nm region assigned to NDI chromophore π–π* transitions polarized along the long axis (z-axis, band-I) [16, 17, 46–49]. Interestingly, the 2D sheets formed from the aqueous solution (H_2O/DMSO: 80/20; v/v) of NDIs **1–3** exhibited significant spectral changes with appreciable bathochromic shifts and hypochromicity along with band broadening at band-I region, suggesting the presence of strong intermolecular NDI–NDI aromatic interactions (Fig. 3a–c). In agreement with absorption studies, fluorescence emission studies of 2D sheets showed the shift of emission spectral features to higher wavelength region compared to emission bands in DMSO solution and displayed tunable broad fluorescence emission properties in the visible spectrum region (400–650 nm). The emission spectra of 2D sheets showed excimer bands (E_{max} = 553 nm for **1** and E_{max} = 537 nm for **3**) and excimer-like emission bands at E_{max} = 472 nm for **2** signifying the effective charge delocalization among the closely packed NDI chromophores (Fig. 3d–f) [16, 17, 46–49]. Therefore, the modulation emission of NDI chromophore from excimer-like (**2**) to excimeric emission (**1** and **3**) was achieved by minute structural mutations in the form of glycine and its derivatives. This is quite remarkable, considering the fact that most of the NDIs and their derivativeness upon aggregation and in solid state exhibit weak or quenched luminescence properties that limited their fluorescence-based applications.

Interestingly, 2D sheets of **1**, **2** and **3** exhibited temperature responsive emission behaviour as shown in the Fig. 4a. **1** showed quite stable excimeric emission at 553 nm in the temperature range of 20–100 °C. A gradual quenching of broad excimer-like emission band of **2** at 472 nm was observed with increase in temperature from 20 to 100 °C. In contrast, **3** exhibited decrease in the excimer emission at 537 nm from 20 to 50 °C and the recovery of excimer emission with further rise in temperature from 50 to 100° C was observed. These contrasting temperature responsive emission behaviours are attributed to thermal disruption of intermolecular NDI–NDI aromatic interactions that led to emissive and nonemissive aggregates [16]. Therefore, 2D sheets of **1**, **2** and **3** are promising materials for solid state temperature sensor systems.

Furthermore time-correlated single photon counting (TCSPC) experiments with nanosecond excitation was performed for **1**, **2** and **3** to understand the emission behaviour of 2D sheets. TCSPC data displayed distinct biexponential decay profiles excimer-like emission (in case of **2**) and excimer emission (for **1** and **3**). NDI **1** at 553 nm and **3** at 537 nm exhibited significantly longer life-times values (4.17 ns, 56 % and 1.11 ns, 44 %) and (1.31 ns 26 % and 3.83 ns, 74 %) respectively. Whereas **2** at 472 nm showed relatively shorter life-times values (0.75 ns, 71 % and 2.8 ns, 30 %) suggesting the formation of ground state excimeric and excimer-like emissive aggregates.

2.3 NMR Studies

In order to probe the hydrogen bonding and aromatic interactions among the NDI molecular units (**1**–**3**) nuclear magnetic resonance (NMR) spectroscopic measurements were performed in DMSO-d_6. The ^{1}H NMR spectra revealed that NDI core aromatic proton chemical shift values were found to be maximum in case of **3** (8.75 ppm) and minimum for **2** (8.71 ppm) whereas that of **1** was found to be moderate (8.74 ppm) (Fig. 5a). The observed NDI core chemical shift values clearly suggest the extent of intermolecular NDI–NDI aromatic overlap and are in the order of **2** > **1** > **3**. Interestingly, **2** displayed the two different chemical shift signals for amide protons, indicating the presence of two kinds of hydrogen bonding interactions among molecular units. To understand the influence of hydrogen bonding and aromatic NDI–NDI interactions on molecular aggregation, we performed concentration dependent ^{1}H NMR studies. All the NDI conjugates (**1**, **2** and **3**) showed upfield shift of NDI aromatic protons to different extent as a function of increasing concentration. **1** showed the upfield shift of NDI aromatic protons ($\Delta\delta_{NDI} = 16.2$ ppb) along with the downfield shift of carboxylic acid protons with $\Delta\delta_{acid} = 45.0$ ppb upon increase in the concentration from 3 to 36 mM (Fig. 5b). **2** and **3** also showed upfield shift of NDI core protons

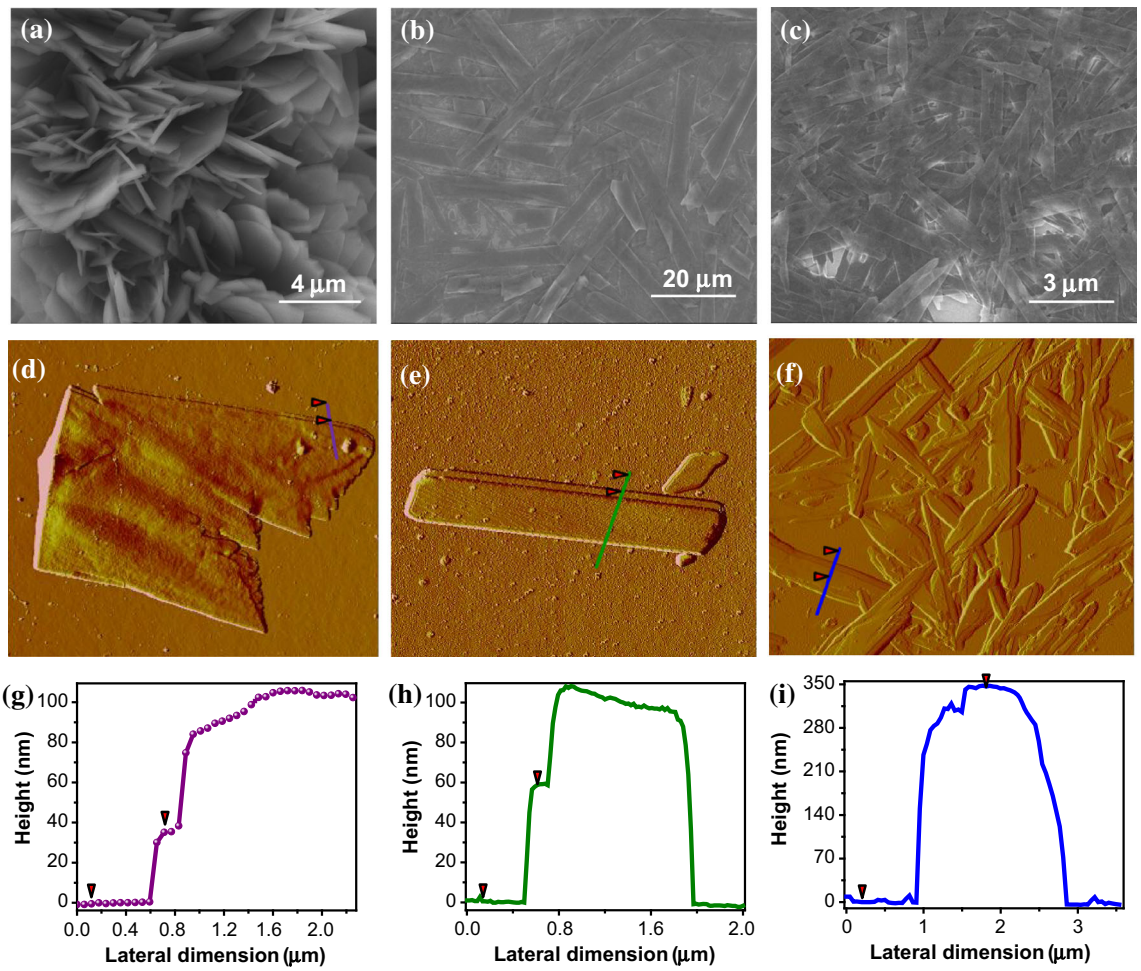

Fig. 2 FESEM image of 2D sheets of **1**(**a**), **2**(**b**) and **3**(**c**). AFM image of **1**(**d**), **2**(**e**) and **3**(**f**) and corresponding AFM height profiles

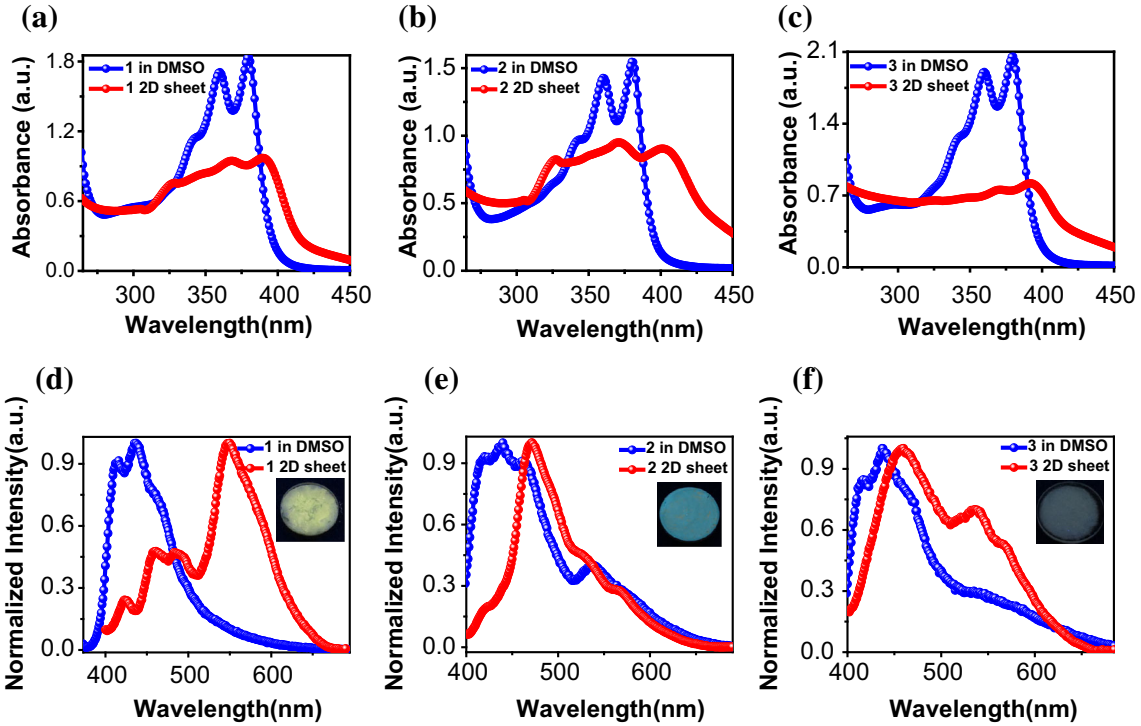

Fig. 3 Photophysical studies of NDIs **1**, **2** and **3**. UV–vis absorption spectra (**a**–**c**) and fluorescence emission spectra (**d**–**f**). *Inset* the photographs of corresponding films on quartz substrate under UV light (365 nm)

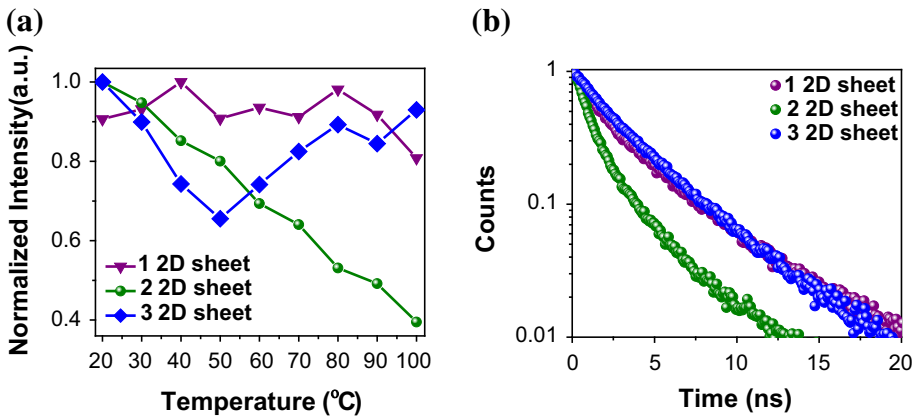

Fig. 4 **a** Temperature dependent fluorescence emission studies (from 20 to 100 °C) of **1** (at 553 nm), **2** (472 nm) and **3** (at 537 nm). **b** TCSPC decay profile of **1** (E_{max} 553 nm), **2** (E_{max} 472 nm) and **3** (E_{max} 537 nm) with a 405 nm excitation

[$\Delta\delta_{NDI}$ = 2.1 ppb for **2** (0.6–9 mM) and $\Delta\delta_{NDI}$ = 10.0 ppb, **3** (3–36 mM)], downfield shift of amide protons in **2** ($\Delta\delta_{amide}$ = 12.0 ppb) and ester protons of **3** ($\Delta\delta_{ester}$ = 3.5 ppb) respectively (Fig. 5c, d). Therefore the observed upfield shift of NDI core protons along with downfield shift of corresponding acid, amide and ester protons as a function of increased concentration confirmed the intermolecular associations due to NDI–NDI aromatic π–π stacking, hydrogen bonding [carboxylic acid (**1**) and amide (**2**)] and CH–O [ester (**3**)] interactions among the molecular units. Noncovalent interactions are sensitive towards temperature and therefore we carried out the variable temperature dependent ^{1}H NMR experiments by increase in temperature from 20 to 100 °C. In contrast to concentration dependent NMR studies, variable temperature dependent ^{1}H NMR experiments showed opposite effect (downfield shift) at the NDI aromatic proton chemical shift region (Fig. 6). With rise in temperature from 20 to 100 °C the NDI core protons of **1**, **2** and **3** displayed the downfield shift with $\Delta\delta_{NDI}$ values 12.5, 6.6 and 9.2 ppb respectively. The downfield shift of NDI core protons is evidently due to the effect of temperature on the NDI–NDI aromatic π–π stacking interactions (Fig. 6a, b and d). Remarkably going from 20 to 100 °C the two amide proton chemical shift signals of **2** (7.75 and 7.25 ppm) are converted into single broad signal centered at 7.15 ppm, revealing the breaking of hydrogen

bonding present among the molecules at higher temperature (Fig. 6c). Overall, concentration and temperature dependent NMR studies revealed the distinct contribution of strong hydrogen bonding and NDI–NDI aromatic interactions in their self-assembly to form 2D sheets with variable shape and size.

Fourier transform infrared spectroscopic (FTIR) measurements further confirmed the presence of hydrogen bonding interactions between molecular units in their respective 2D sheets. **1** and **2** displayed broad carboxylic acid stretching frequency at 3,600–3,800 cm^{-1} and amide stretching frequency at 3,100–3,400 cm^{-1} respectively.

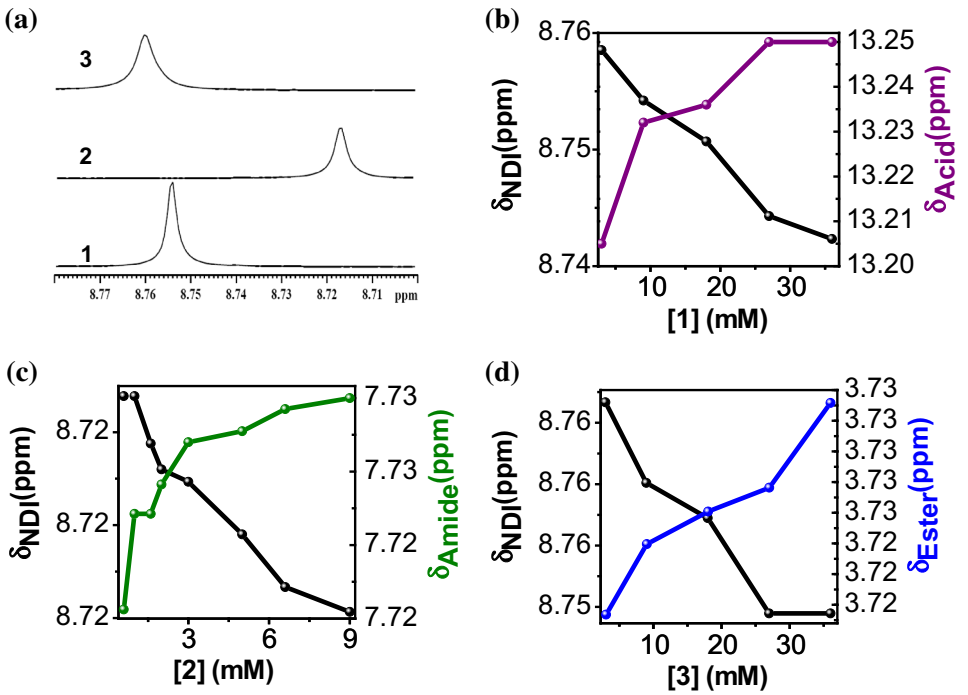

Fig. 5 **a** ^{1}H NMR spectra of **1**, **2** and **3** at NDI region (8.8–8.7 ppm). **b** Plot of concentration versus NDI and carboxylic acid proton chemical shifts of **1**. **c** Plot of concentration versus NDI and amide proton chemical shifts of **2**. **d** Plot of concentration versus NDI and ester proton chemical shifts of **3**

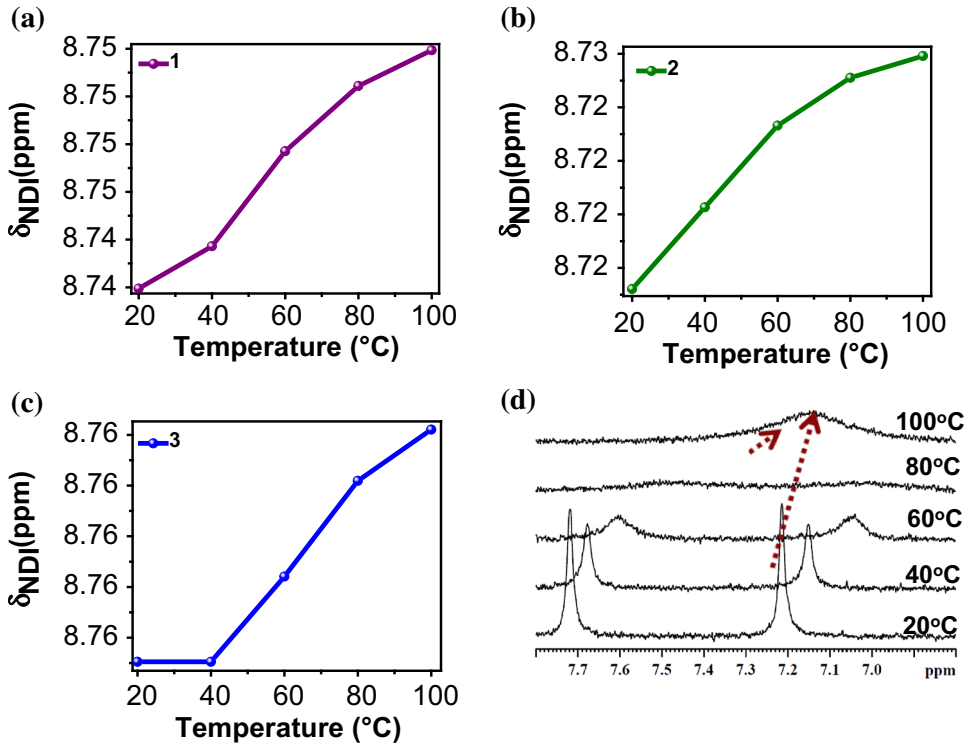

Fig. 6 Plot of NDI proton chemical shift as a function of temperature for **1** (**a**), **2** (**b**) and **3** (**c**). **d** ^{1}H NMR spectra of **2** in the amide region (6.8–7.8 ppm)

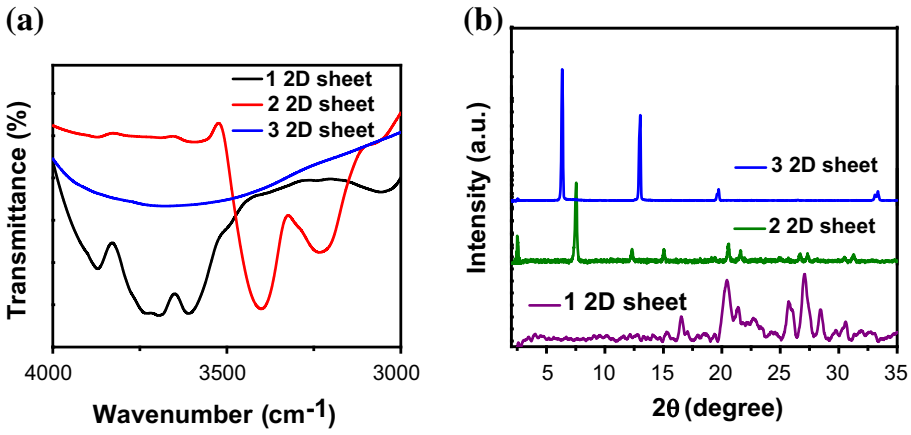

Fig. 7 **a** FT-IR spectra of 2D sheets of **1**–**3** in the region 3,000–4,000 cm^{-1}. **b** PXRD diffraction patterns of **1**–**3** 2D sheets at 25 °C

Whereas NDI **3** did not show any characteristic band in the 3,000–4,000 cm^{-1} region (Fig. 7a). Furthermore, the powder X-ray diffraction (PXRD) data showed sharp and intense reflections in the low-angle as well as higher-angle regions for all the 2D sheets of **1**, **2** and **3**. This data suggest crystalline arrangement of molecules and the preferred orientation of molecular planes within the 2D sheets (Fig. 7b). The reflections at low-angle ($2\theta = 20°$–$35°$) corresponded to intermolecular π-stacking distances and hydrogen bonding distances between the molecules within the 2D sheets of **1**, **2** and **3** respectively. Furthermore, we carried out FTIR and PXRD measurements after annealing the 2D sheets of **1**, **2** and **3** at 100 °C and the results were compared with that of as-prepared samples. FT-IR data clearly indicated the absence of any significant modifications in the 2D sheets of **1**, **2** and **3** after annealing process, as the samples displayed unmodified stretching frequencies (Figure S10–S12). Although PXRD data exhibited relatively distinct patterns upon annealing at 100 °C signifying molecular reorganization within the 2D sheets (Figure S14). Therefore the observed changes in the photoluminenesence properties of 2D sheets upon heating are purely due to the reorganization of self-assembly processes but not the chemical modification.

3 Conclusions

We demonstrated a bioinspired nanoarchitectonics design strategy to construct 2D sheets of NDIs by controlling their self-assembly propensity. Subtle changes in the form of structural mutations of glycine derivatives (carboxylic acid, amide and ester respectively) in NDIs **1**–**3** led to 2D nanosheets with distinct but well-defined shapes in terms of length, width and thickness. The spectroscopic (photophysical, concentration and temperature dependent NMR and IR), microscopy (AFM and FESEM) and powder XRD analysis suggested that the variable strength and directionality of intermolecular hydrogen bonding interactions among the structural units of glycine functionalized NDI are responsible for the observed variable shape and size of 2D sheets of **1**–**3**. In addition, the variable shape and size of 2D sheets of NDIs **1**–**3** is also attributed to intermolecular hydrogen bonding interactions controlled NDI–NDI aromatic interactions. Remarkably, 2D sheets of NDIs **1**–**3** exhibited emission in the longer wavelength (visible) region with high Stoke shift signifying the potential of these materials for fluorescence-based applications. Interestingly, 2D sheets showed temperature responsive emission properties and are promising materials for solid state temperature sensor systems. NMR and IR studies confirmed the presence of strong and distinct hydrogen bonding and NDI–NDI aromatic interactions with in the self-assembled 2D sheets. PXRD diffraction patterns revealed highly crystalline molecular organization and preferred molecular planes orientations within the 2D sheets. Overall, our nanoarchitectonics approach based on the bioinspired strategy in the form of minute structural mutations of glycine is capable of controlling the self-assembly of promising n-type organic semiconductor NDI into 2D sheets with tunable shape, size and interesting solid state optical properties. We believe that our bioinspired nanoarchitectonics design strategy is highly useful in controlling the noncovalent interactions of functional aromatic molecules, which in turn give rise to desirable crystalline molecular packing and interesting optical properties important for wide range of applications from materials to biomedicine [1–5].

Acknowledgments The authors thank Prof. C. N. R. Rao for constant support and encouragement, JNCASR, Department of Biotechnology (DBT)-Innovative Young Biotechnologist Award (IYBA) (Grant BT/03/IYBA/2010), India for financial support, Sheikh Saqr Laboratory (SSL), ICMS, JNCASR for Sheikh Saqr Career Award Fellowship to T.G.

References

1. M.B. Avinash, T. Govindaraju, Nanoscale **6**, 13348–13369 (2014)
2. K. Ariga, K. Kawakami, M. Ebara, Y. Kotsuchibashi, Q. Ji, J.P. Hill, New J. Chem. **38**, 5149–5163 (2014)
3. K. Ariga, A. Vinu, Y. Yamauchi, Q. Ji, J.P. Hill, Bull. Chem. Soc. Jpn **85**, 1–32 (2013)
4. M. Aono, Y. Bando, K. Ariga, Adv. Mater. **24**, 150–151 (2012)
5. T. Govindaraju, M.B. Avinash, Nanoscale **4**, 6102–6117 (2012)
6. C.N.R. Rao, A.K. Sood, K.S. Subrahmanyam, A. Govindaraj, Angew. Chem. Int. Ed. **48**, 7752–7777 (2009)
7. A.K. Geim, K.S. Novoselov, Nat. Mater. **6**, 183–191 (2007)
8. X. Peng, L. Peng, C. Wu, Y. Xie, Chem. Soc. Rev. **43**, 3303–3323 (2014)
9. C.N.R. Rao, U. Maitra, U.V. Waghmare, Chem. Phys. Lett. **609**, 172–183 (2014)
10. C.N.R. Rao, H.S.S. Ramakrishna Matte, U. Maitra, Angew. Chem. Int. Ed. **52**, 13162–13185 (2013)
11. F. Geng, R. Ma, A. Nakamura, K. Akatsuka, Y. Ebina, Y. Yamauchi, N. Miyamoto, Y. Tateyama, T. Sasaki, Nat. Commun. **4**, 1632–1638 (2013)
12. M. Osada, T. Sasaki, Adv. Mater. **24**, 210–228 (2012)
13. J. Liu, X.-W. Liu, Adv. Mater. **24**, 4097–4111 (2012)
14. R. Mas-Balleste, C. Gomez-Navarro, J. Gomez-Herrero, F. Zamora, Nanoscale **3**, 20–30 (2011)
15. T. Jiang, C. Xu, Y. Liu, Z. Liu, J.S. Wall, X. Zuo, T. Lian, K. Salaita, C. Ni, D. Pochan, V.P. Conticello, J. Am. Chem. Soc. **136**, 4300–4308 (2014)
16. K. Ariga, Y. Yamauchi, G. Rydzek, Q. Ji, Y. Yonamine, K.C.W. Wu, J.P. Hill, Chem. Lett. **43**, 36–68 (2014)
17. K. Ariga, Y. Yamauchi, T. Mori, J.P. Hill, Adv. Mater. **25**, 6477–6512 (2013)
18. K.T. Nam, S.A. Shelby, P.H. Choi, A.B. Marciel, R. Chen, L. Tan, T.K. Chu, R.A. Mesch, B.-C. Lee, M.D. Connolly, C. Kisielowski, R.N. Zuckermann, Nat. Mater. **9**, 454–460 (2010)
19. J. Sakamoto, J. van Heijst, O. Lukin, A.D. Schlüter, Angew. Chem. Int. Ed. **48**, 1030–1069 (2009)
20. U.B. Sleytr, P. Messner, D. Pum, M. Sára, Angew. Chem. Int. Ed. **38**, 1034–1054 (1999)
21. X. Zhuang, Y. Mai, D. Wu, F. Zhang, X. Feng, Adv. Mater. (2014). doi:10.1002/adma.201401857
22. M. Pandeeswar, H. Khare, S. Ramakumar, T. Govindaraju, RSC Adv. **4**, 20154–20163 (2014)
23. M. Pandeeswar, T. Govindaraju, RSC Adv. **3**, 11459–11462 (2013)
24. N. Narayanaswamy, M.B. Avinash, T. Govindaraju, New J. Chem. **37**, 1302–1306 (2013)
25. J. Xu, G. Wu, Z. Wang, X. Zhang, Chem. Sci. **3**, 3227–3230 (2012)
26. M.B. Avinash, T. Govindaraju, Adv. Funct. Mater. **21**, 3875–3882 (2011)
27. T. Govindaraju, M. Pandeeswar, K. Jayaramulu, G. Jaipuria, H.S. Atreya, Supramol. Chem. **23**, 487–492 (2011)
28. K. Ariga, J.P. Hill, Y. Wakayama, Phys. Status Solidi A **205**, 1249–1257 (2008)
29. Z. Wang, Z. Li, C.J. Medforth, J.A. Shelnutt, J. Am. Chem. Soc. **129**, 2440–2441 (2007)
30. R. Davis, R. Berger, R. Zentel, Adv. Mater. **19**, 3878–3881 (2007)
31. D. Shukla, S.F. Nelson, D.C. Freeman, M. Rajeswaran, W.G. Ahearn, D.M. Meyer, J.T. Carey, Chem. Mater. **20**, 7486–7491 (2008)
32. R. Österbacka, C.P. An, X.M. Jiang, Z.V. Vardeny, Science **287**, 839–842 (2000)
33. X. Zhan, A. Facchetti, S. Barlow, T.J. Marks, M.A. Ratner, M.R. Wasielewski, S.R. Marder, Adv. Mater. **23**, 268–284 (2011)
34. T. Weil, T. Vosch, J. Hofens, K. Peneva, K. Mullen, Angew. Chem. Int. Ed. **49**, 9068–9093 (2010)
35. J.E. Anthony, A. Facchetti, M. Heeney, S.R. Marder, X. Zhan, Adv. Mater. **22**, 3876–3892 (2010)
36. M.B. Avinash, T. Govindaraju, Adv. Mater. **24**, 3905–3922 (2012)
37. J.B. Bodapati, H. Icil, Photochem. Photobiol. Sci. **10**, 1283–1293 (2011)
38. Y. Takashima, V.M. Martinez, S. Furukawa, M. Kondo, S. Shimomura, H. Uehara, M. Nakahama, K. Sugimoto, S. Kitagawa, Nat. Commun. **2**, 168 (2010)
39. V. Tumiatti, A. Milelli, A. Minarini, M. Micco, A. Gasperi Campani, L. Roncuzzi, D. Baiocchi, J. Marinello, G. Capranico, M. Zini, C. Stefanelli, C. Melchiorre, J. Med. Chem. **52**, 7873–7877 (2009)
40. S.V. Bhosale, C.H. Jani, S.J. Langford, Chem. Soc. Rev. **37**, 331–342 (2008)
41. S.K.M. Nalluri, C. Berdugo, N. Javid, P.W.J.M. Frederix, R.V. Ulijn, Angew. Chem. Int. Ed. **53**, 5882–5887 (2014)
42. S. Manchineella, V. Prathyusha, U. Deva Priyakumar, T. Govindaraju, Chem. Eur. J. **19**, 16615–16624 (2013)
43. M. Pandeeswar, M.B. Avinash, T. Govindaraju, Chem. Eur. J. **18**, 4818–4822 (2012)
44. G.G. Holman, M. Zewail-Foote, A.R. Smith, K.A. Johnson, B.L. Iverson, Nature Chem. **3**, 875–881 (2011)
45. D.R. Trivedi, Y. Fujiki, N. Fujita, S. Shinkai, K. Sada, Chem. Asian J. **4**, 254–261 (2009)
46. S.H. Kim, J.R. Parquette, Nanoscale **4**, 6940–6947 (2012)
47. G.D. Pantoş, P. Pengo, J.K.M. Sanders, Angew. Chem. Int. Ed. **46**, 194–197 (2007)
48. N. Ashkenasy, W.S. Horne, M.R. Ghadiri, Small **2**, 99–102 (2006)
49. M. Tomasulo, D.M. Naistat, A.J.P. White, D.J. Williams, F.I.M. Raymo, Tetrahedron Lett. **46**, 5695–5698 (2005)